Normal Modes in an Overmoded Circular Waveguide Coated with Lossy Material

CHOON SAE LEE, STUDENT MEMBER, IEEE, SHUNG-WU LEE, FELLOW, IEEE, AND SHUN-LIEN CHUANG, MEMBER, IEEE

Abstract —**The normal modes in an overmoded waveguide coated with a lossy material are analyzed, particularly for their attenuation properties as a function of coating material, layer thickness, and frequency. When the coating material is not too lossy, the low-order modes are highly attenuated even with a thin layer of coating. This coated guide serves as a mode suppressor of the low-order modes, which can be particularly useful for reducing the radar cross section (RCS) of a cavity structure such as a jet engine inlet. When the coating material is very lossy, low-order modes fall into two distinct groups: highly and lowly attenuated modes. However, as a/λ (a = radius of the cylinder; λ = the free-space wavelength) increases, the separation between these two groups becomes less distinctive. The attenuation constants of most of the low-order modes become small and decrease as a function of λ^2/a^3.**

I. Introduction

IN MANY APPLICATIONS, it is desirable to line the wall of a conventional circular waveguide by a layer of dielectric or magnetic material. With proper design, the lining can significantly alter the modal fields in the waveguide, so as to achieve either less attenuation or more attenuation for certain modes. The past studies of this problem are mostly connected with microwave/infrared transmission over a long distance [1]–[5]. Two assumptions are usually made:

1) The waveguide diameter is very large in terms of wavelength (overmoded waveguide); and

2) The coating material is either nearly lossless [2]–[4] or very lossy [5].

These assumptions simplify the theoretical analysis and oftentimes bring out a clearer physical picture. Nevertheless, in many practical situations, these assumptions are too restrictive. A more general analysis of the coated circular waveguide is needed.

It is the purpose of this paper to fill in this need. Instead of using the perturbation theory [2], [3], [5], transmission-line model [1]–[4], or asymptotic theory [6], we solve the modal characteristic equation of a coated circular waveguide exactly by a numerical method. This is feasible because of today's fast computers and efficient subroutines for calculating Bessel functions with a complex argument.

The organization of the paper is as follows: First, an overview of the normal modes in a coated circular waveguide in comparison with those in an uncoated waveguide is presented. In Section III, the exact characteristic equation for the normal modes in a circular waveguide coated with a lossy material is given. Three types of normal modes, i.e., the inner mode, the surface mode, and the interface mode, are discussed, along with their approximate solutions. Numerical results and potential applications are discussed in Section IV.

Manuscript received September 16, 1985; revised February 11, 1986. This work was supported in part by NASA under Contract NAG3-475.

The authors are with the Electromagnetics Laboratory, University of Illinois, Urbana IL 61801.

IEEE Log Number 8608335.

II. Overview of Modal Fields in a Coated Circular Waveguide

Before presenting detailed numerical results, it is beneficial to explain some unique features of the coated waveguide, which are absent in the conventional uncoated waveguide. Fig. 1 shows a circular waveguide with a perfectly conducting wall, uniformly coated with a material of permittivity $\epsilon_2\epsilon_0$ and permeability $\mu_2\mu_0$. Both ϵ_2 and μ_2 can be complex, with their negative imaginary parts representing material losses for the present exp $(j\omega t)$ time convention. The medium in Region I is assumed to be air, i.e., permittivity ϵ_0 and permeability μ_0. Our problem at hand is to study the normal modes in such a waveguide. In this section, the coating material is assumed to be lossless.

A. Mode Classification

In an uncoated waveguide, the normal modes are either TE or TM with respect to z. Here index m describes the azimuthal variation in the form of $\sin m\phi$ or $\cos m\phi$, whereas index n describes the radial distribution in the form of $J_m(k_{\rho n}\rho)$ or $J'_m(k_{\rho n}\rho)$. In the ascending order of their cutoff frequencies, the dominant modes are

$$TE_{11}, TM_{01}, TE_{21}, TM_{11}/TE_{01}, \cdots .$$

When the waveguide is coated with a dielectric layer, there are no longer pure TE or TM modes. The modes are commonly classified into HE_{mn} and EH_{mn} modes in such a way that, in the limiting case of a vanishingly thin coating [7]

$$HE_{mn} \rightarrow TE_{mn}, \quad \text{and} \quad EH_{mn} \rightarrow TM_{mn}.$$

There exist three special cases where $HE_{mn}(EH_{mn})$ becomes identically or approximately $TE_{mn}(TM_{mn})$, namely:

(i) Circularly symmetrical modes ($m = 0$) such as TE_{0n} and TM_{0n}.

(ii) All modes at frequencies near their cutoff frequencies [8], [9].

0018-9480/86/0700-0773$01.00 ©1986 IEEE

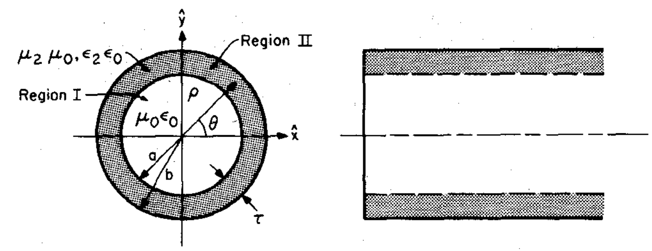

Fig. 1. A coated circular waveguide.

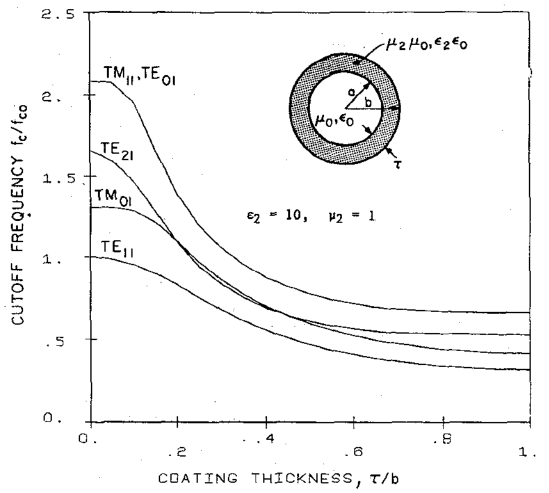

Fig. 2. The cutoff frequencies in a dielectric-coated waveguide ($\epsilon_2 = 10$, $\mu_2 = 1$) normalized to that of the TE_{11} mode in an empty guide (f_{co}) as a function of coating thickness.

(iii) The low-order modes in an overmoded waveguide coated with a lossless material, (in this limit $HE_{mn} \to TM_{mn}$, and $EH_{mn} \to TE_{mn}$).

B. Cutoff Frequencies

Near the cutoff frequency, the normal mode is either quasi-TE or TM. In Figs. 2 and 3, we plot the cutoff frequencies f_c's of the normal modes in a coated circular guide as a function of layer thickness τ. f_c is normalized with respect to f_{co}, which is the cutoff frequency of the dominant TE_{11} mode in an empty guide of radius a, and is given by

$$f_{co} = \frac{1.84118c}{2\pi a}$$

where c is the speed of light in free space. Fig. 2 shows the modal inversion between the TM_{01} and TE_{21}, which has been previously reported [8], [9]. However, the modal inversion between those two modes is not evident if the coating is of a magnetic material ($\mu_2 \neq 1$) instead of a dielectric material (Fig. 3). Coating reduces the cutoff frequencies of the normal modes, especially for the magnetic-coated waveguide. This is due to the fact that, with coating, the modal field distribution tends to concentrate near the air-material interface. Note also that the degeneracy between the TM_{11} and TE_{01} modes near their cutoff frequencies is not removed by the dielectric coating (see Appendix I), but the degeneracy can be removed by the magnetic coating. The near degeneracy of the TE_{01} mode with the TM_{11} mode in a dielectric-coated guide can cause a serious problem for a long-distance communication utilizing the lowly attenuating TE_{01} mode, because there may be a large mode conversion due to a strong coupling between these two modes [2]–[4]. The magnetic coating can be very useful in this application.

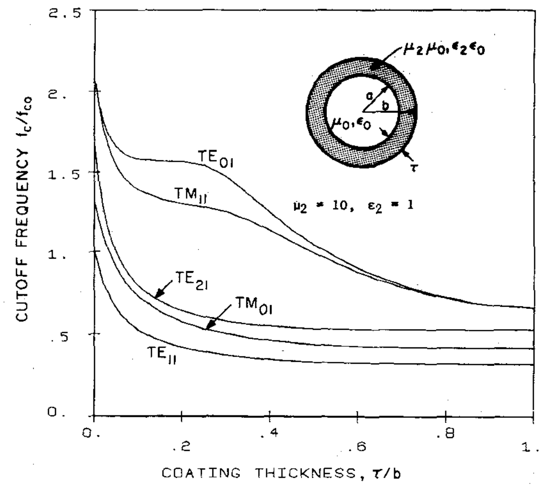

Fig. 3. The cutoff frequencies in a magnetic-coated waveguide ($\mu_2 = 10$, $\epsilon_2 = 1$) normalized to that of the TE_{11} mode in an empty guide (f_{co}) as a function of coating thickness.

C. Modal Propagation Constant and Power Distribution

When the coating thickness is small in terms of the free-space wavelength ($\tau/\lambda \ll 1$), the modal field distribution in the air region and the propagation constant are not much perturbed. As the coating thickness is increased in the manner

$$\tau/\lambda \to \infty, \qquad \text{for a fixed value of } a$$

the low-order modes approach, one by one, their counterparts in the parallel-plate waveguide. More precisely, the HE_{mn} modes in a coated circular waveguide approach those modes in a parallel-plate waveguide formed by a perfect magnetic conductor (PMC) and perfect electric conductor (PEC) as sketched in Fig. 4(a). The EH_{mn} modes approach those modes in a parallel-plate waveguide formed by two PEC's as shown in Fig. 4(b).

The propagation constant k_z and modal power distribution of the dominant HE_{11} mode in a guide coated with a lossless dielectric material ($\epsilon_2 = 10$, $\mu_2 = 1$) are shown in Figs. 5 and 6. When the coating thickness is small ($\tau'/\lambda = \tau/\lambda_2 < 0.05$, where $\lambda_2 = \lambda/\sqrt{\epsilon_2\mu_2}$ = wavelength in Region II), the transverse wave number $k_{\rho 1}$ in Region I defined by

$$k_{\rho 1} = \sqrt{k_0^2 - k_z^2}$$

is real, where $k_0 = 2\pi/\lambda$, and both propagation constant and its power-intensity distribution are very similar to those of an empty guide. When the coating thickness τ is much larger than $0.05\lambda_2$, $k_{\rho 1}$ is imaginary and its magnitude approaches $k_0\sqrt{\epsilon_2\mu_2 - 1}$. Consequently, the modal power distribution is largely concentrated in the dielectric layer (Region II). In Fig. 6, the total power carried by the

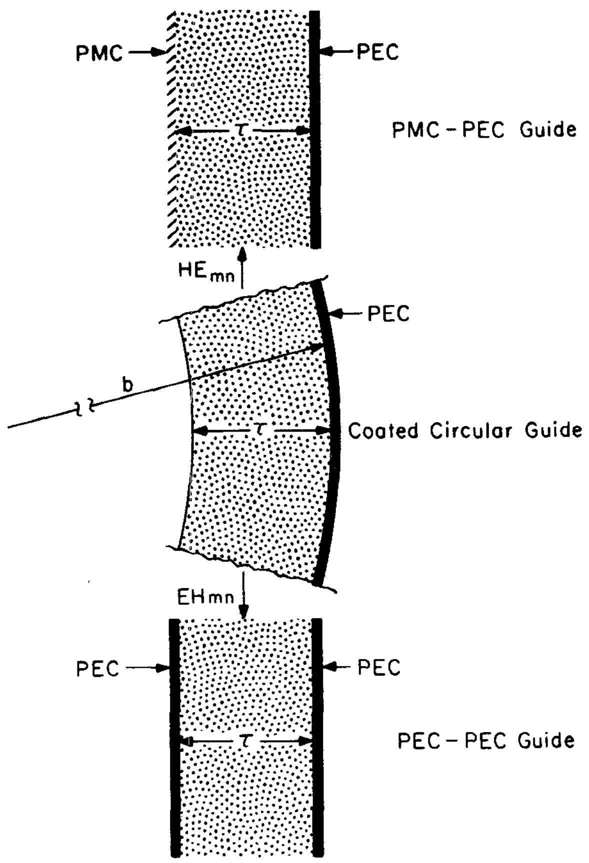

Fig. 4. Mode transition in a coated circular guide at the high-frequency limit. The HE_{mn} modes approach modes in a PMC-PEC guide and the EH_{mn} approach modes in PEC-PEC guide.

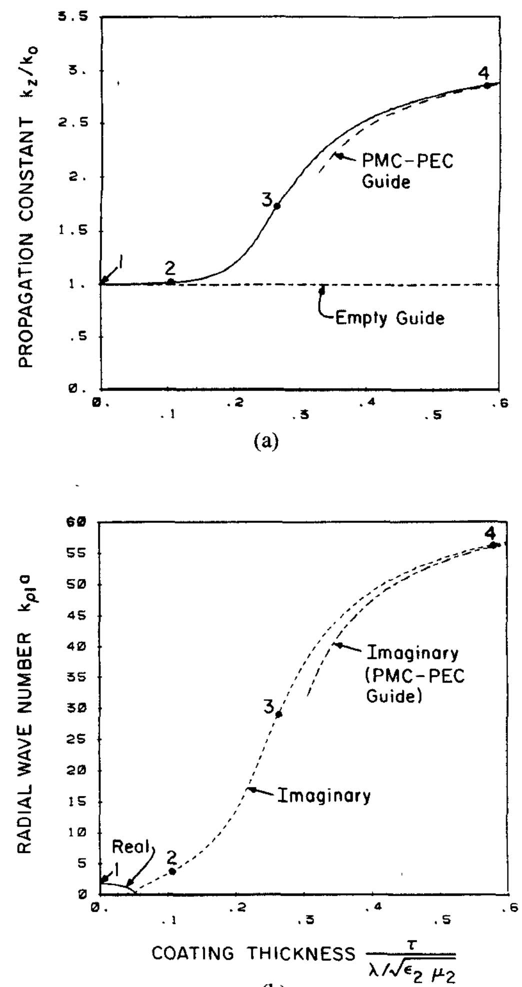

Fig. 5. (a) Normalized propagation constant and (b) radial wave number ($k_{\rho 1}a$) of the HE_{11} mode in a dielectric-coated waveguide ($\epsilon_2 = 10$, $\mu_2 = 1$) as a function of the coating thickness in "effective" wavelength ($\tau' = \tau\sqrt{\epsilon_2\mu_2}/\lambda$). The power distributions for the four marked points are shown in Fig. 6. The approximate solution of the surface mode using the two-slab model is also shown (see Section III).

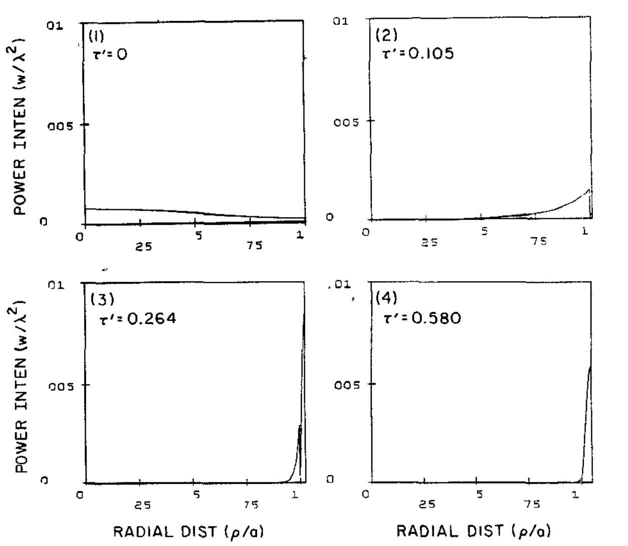

Fig. 6. Normalized angle-averaged power distribution in watts/λ^2 as a function of radial distance in a dielectric-coated waveguide ($\epsilon_2 = 10$, $\mu_2 = 1$) with four different coating thicknesses. The corresponding points for these diagrams are marked in Fig. 5 ($\tau' = \tau\sqrt{\epsilon_2\mu_2}/\lambda$).

HE_{11} mode is normalized to 1 W. In case (4) of Fig. 6, more than 99 percent of the power is confined in the dielectric layer, despite the fact that the dielectric layer ($1.06 < \rho/a < 1$) covers only 12 percent of the waveguide cross section.

Figs. 7 and 8 are similar to Figs. 5 and 6 except that the coating material is magnetic ($\mu_2 = 10$ and $\epsilon_2 = 1$). It is most interesting to observe that the transition point where k_z becomes imaginary occurs at a much smaller coating thickness ($\tau = 0.05\lambda_2$ in Fig. 5 and $\tau = 0.005\lambda_2$ in Fig. 7). Thus, in applications where large field concentration in the material layer is desired, the magnetic coating is more effective (more discussion is given in Section IV).

It is worthwhile to note that the normal mode at the transition point is not TEM even though the radial wave number vanishes (see Appendix II). Thus, both the hybrid-mode method and the techniques for TEM modes fail to provide the modal fields at the transition point. Only the direct method, as discussed in Appendix II, is applicable in this case.

D. Transverse-Field Distribution

The transverse fields of the five lowest-order modes in an uncoated circular guide and in a coated (dielectric and magnetic) circular guide at the cutoff frequencies and the high-frequency limits are shown in Fig. 9. The TE (TM) modes in a circular guide at the cutoff frequencies do not

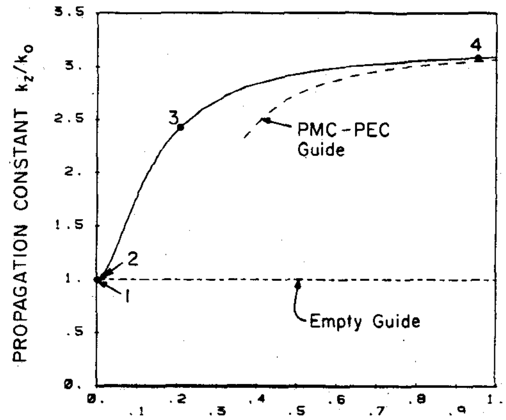

(a)

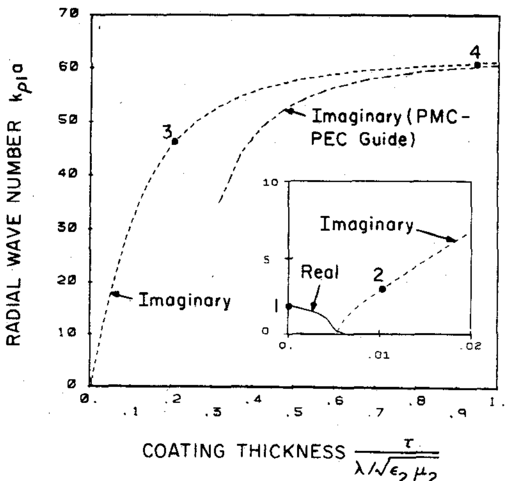

(b)

Fig. 7. (a) Normalized propagation constant and (b) radial wave number ($k_{\rho 1}a$) of the HE_{11} mode in a magnetic-coated waveguide ($\mu_2 = 10$, $\epsilon_2 = 1$) as a function of the lining thickness in "effective" wavelength ($\tau' = \tau\sqrt{\epsilon_2\mu_2}/\lambda$). The power distributions of the four marked points are shown in Fig. 8. The approximate solution of the surface mode using the two-slab model is also shown (see Section III).

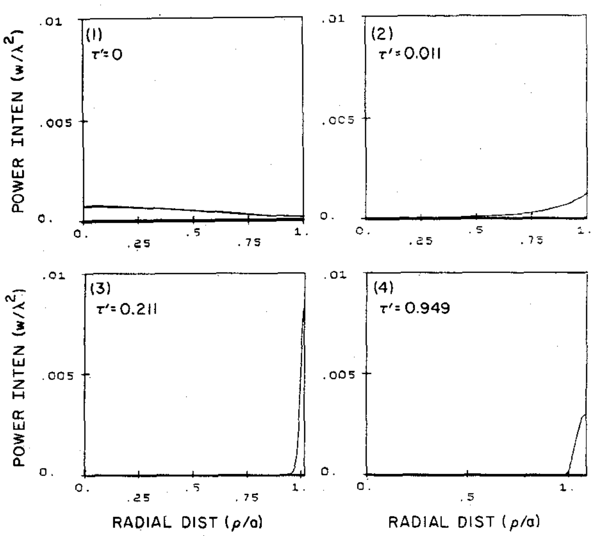

Fig. 8. Normalized angle-averaged power distribution in watts/λ^2 as a function of radial distance in a magnetic-coated waveguide ($\mu_2 = 10$, $\epsilon_2 = 1$) with four different coating thicknesses. The corresponding points for these diagrams are marked in Fig. 7 ($\tau' = \tau\sqrt{\epsilon_2\mu_2}/\lambda$).

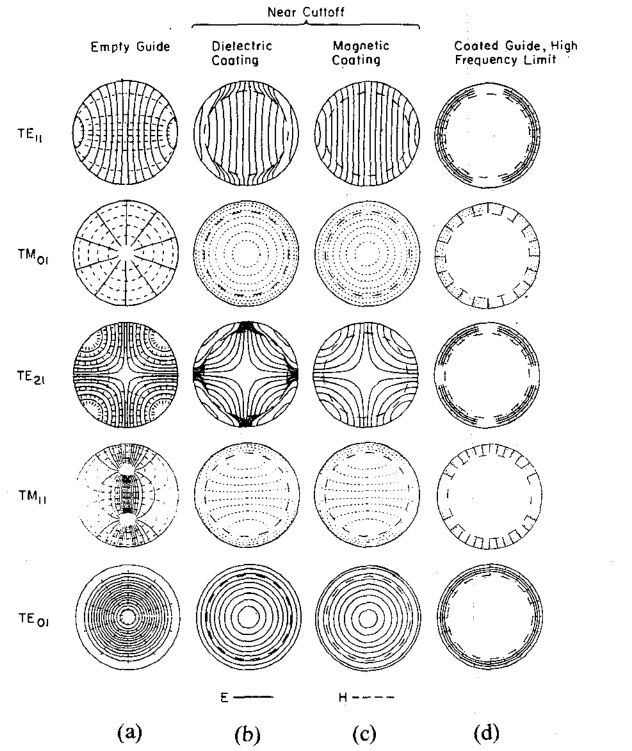

Fig. 9. Transverse field distributions of the normal modes in (a) empty guide, (b) dielectric-coated guide at cutoff frequencies, (c) magnetic-coated guide at cutoff frequencies and (d) coated guide at the high-frequency limit.

have transverse magnetic (electric) fields, which are not shown in the diagrams. We notice that the nonvanishing fields at the cutoff frequencies are similar to those in an uncoated guide. At high frequency, the fields are confined within the coated region, as shown in the diagrams where the blank space indicates that the fields are negligible.

III. Modal Characteristic Equations, Fields, and Classification

The general problem is shown in Fig. 1. Here both the permittivity $\epsilon_2\epsilon_0$ and permeability $\mu_2\mu_0$ of the coating material are allowed to be complex. The characteristic equation for the propagation constant k_z of a normal mode is well known [10], [11], and we list the final expression, which is solved numerically using Müller's method (available in International Mathematical Statistical Libraries subroutines)

$$k_{\rho 1}^2\left[F_1'(a) - \epsilon_2 \frac{F_1(a)F_3'(a)}{F_3(a)}\frac{k_{\rho 1}}{k_{\rho 2}}\right]$$

$$\cdot\left[F_1'(a) - \mu_2 \frac{F_1(a)F_4'(a)}{F_4(a)}\frac{k_{\rho 1}}{k_{\rho 2}}\right]$$

$$-\left[k_z m/(k_0 a)\right]^2 F_1^2(a)\left[1-(k_{\rho 1}/k_{\rho 2})^2\right]^2 = 0 \quad (1a)$$

where

$$k_{\rho 1}^2 + k_z^2 = k_0^2 \tag{1b}$$

$$k_{\rho 2}^2 + k_z^2 = \epsilon_2 \mu_2 k_0^2 \tag{1c}$$

$$F_1(\rho) = J_m(k_{\rho 1}\rho), \quad F_1'(\rho) = J_m'(k_{\rho 1}\rho) \tag{1d}$$

$$F_3(\rho) = J_m(k_{\rho 2}\rho) N_m(k_{\rho 2}b) - N_m(k_{\rho 2}\rho) J_m(k_{\rho 2}b) \tag{1e}$$

$$F_3'(\rho) = J_m'(k_{\rho 2}\rho) N_m(k_{\rho 2}b) - N_m'(k_{\rho 2}\rho) J_m(k_{\rho 2}b) \tag{1f}$$

$$F_4(\rho) = J_m(k_{\rho 2}\rho) N_m'(k_{\rho 2}b) - N_m(k_{\rho 2}\rho) J_m'(k_{\rho 2}b) \tag{1g}$$

$$F_4'(\rho) = J_m'(k_{\rho 2}\rho) N_m'(k_{\rho 2}b) - N_m'(k_{\rho 2}\rho) J_m'(k_{\rho 2}b). \tag{1h}$$

Here $k_{\rho 1}$ and $k_{\rho 2}$ are the radial wave vectors of regions I and II, respectively; ω is the angular frequency; $k_0 = 2\pi/\lambda$; and a and b are the radii of the air region and the conducting cylinder, respectively. J_m is the Bessel function and N_m is the Neumann function of order m. The prime indicates differentiation with respect to argument. The modal fields are given by

$$E_\rho^I = -\left[(Ak_z/k_0)F_1'(\rho) + (Bm/k_{\rho 1}\rho)F_1(\rho)\right]\cos m\phi \tag{2a}$$

$$E_\rho^{II} = -\left[(Ck_z/k_2)F_3'(\rho) + (Dm/k_{\rho 2}\rho)F_4(\rho)\right]\cos m\phi \tag{2b}$$

$$E_\phi^I = \left[\{Ak_z m/(k_0 k_{\rho 1}\rho)\}F_1(\rho) + BF_1'(\rho)\right]\sin m\phi \tag{2c}$$

$$E_\phi^{II} = \left[\{Ck_z m/(k_2 k_{\rho 2}\rho)\}F_3(\rho) + DF_4'(\rho)\right]\sin m\phi \tag{2d}$$

$$E_z^I = -j(Ak_{\rho 1}/k_0)F_1(\rho)\cos m\phi \tag{2e}$$

$$E_z^{II} = -j(Ck_{\rho 2}/k_2)F_3(\rho)\cos m\phi \tag{2f}$$

$$H_\rho^I = -Y_0\left[(Am/k_{\rho 1}\rho)F_1(\rho) + (Bk_z/k_0)F_1'(\rho)\right]\sin m\phi \tag{2g}$$

$$H_\rho^{II} = -Y_2\left[(Cm/k_{\rho 2}\rho)F_3(\rho) + (Dk_z/k_2)F_4'(\rho)\right]\sin m\phi \tag{2h}$$

$$H_\phi^I = -Y_0\left[AF_1'(\rho) + \{Bk_z m/(k_0 k_{\rho 1}\rho)\}F_1(\rho)\right]\cos m\phi \tag{2i}$$

$$H_\phi^{II} = -Y_2\left[CF_3'(\rho) + \{Dk_z m/(k_2 k_{\rho 2}\rho)\}F_4(\rho)\right]\cos m\phi \tag{2j}$$

$$H_z^I = -jY_0(Bk_{\rho 1}/k_0)F_1(\rho)\sin m\phi \tag{2k}$$

$$H_z^{II} = -jY_2(Dk_{\rho 2}/k_2)F_4(\rho)\sin m\phi. \tag{2l}$$

The convention of $\exp[j(\omega t - k_z z)]$ is understood and omitted; superscripts I and II indicate Regions I and II (Fig. 1), and subscripts ρ, ϕ, and z indicate the radial, angular, and propagation-directional components of the fields, respectively; $k_2 = \sqrt{\epsilon_2\mu_2}\,k_0$; and Y_0 is the free-space admittance, $\sqrt{\epsilon_0/\mu_0}$ and $Y_2 = Y_0\sqrt{\epsilon_2/\mu_2}$. A, B, C, and D are the constants, which are determined by the boundary conditions and the normalization requirement. Those constants are related by

$$C = A\sqrt{\epsilon_2\mu_2}\,k_{\rho 1}F_1(a)/\left[k_{\rho 2}F_3(a)\right] \tag{3}$$

$$D = B\mu_2 k_{\rho 1}F_1(a)/\left[k_{\rho 2}F_4(a)\right] \tag{4}$$

$$\frac{B}{A} = -\frac{k_0 k_{\rho 1} a\left[F_1'(a)/F_1(a) - \epsilon_2 k_{\rho 1}F_3'(a)/\{k_{\rho 2}F_3(a)\}\right]}{k_z m\left[1-(k_{\rho 1}/k_{\rho 2})^2\right]} \quad (m \neq 0) \tag{5}$$

$$\left(\left|\frac{B}{A}\right| \ll 1 \text{ for "quasi" TM modes}\right).$$

Equation (5) can also be written as

$$\frac{A}{B} = -\frac{k_0 k_{\rho 1} a\left[F_1'(a)/F_1(a) - \mu_2 k_{\rho 1}F_4'(a)/\{k_{\rho 2}F_4(a)\}\right]}{k_z m\left[1-(k_{\rho 1}/k_{\rho 2})^2\right]} \quad (m \neq 0) \tag{6}$$

$$\left(\left|\frac{A}{B}\right| \ll 1 \text{ for "quasi" TE modes}\right)$$

and the elimination of A and B from (5) and (6) gives the characteristic equation (1). There is no mode coupling between the TE and TM modes for $m = 0$. Thus, $A = 0$ and $B = 1$ for the TM_{0n} modes, and $A = 1$ and $B = 0$ for the TE_{0n} modes. We note that there are two degenerate modes for each angular mode index m except $m = 0$. In the above expression of the fields, we have arbitrarily chosen one of those two modes.

There are three types of normal modes in an overmoded waveguide coated with a lossy material. The properties of these modes are explained below along with the approximate propagation constants and field distributions.

A. Inner Mode

When the coating material is sufficiently lossy and a/λ is large, most of the low-order modes become inner modes. The field distributions of these modes are mostly confined in the air region. In the limit as a/λ becomes infinite, the characteristic equation is simplified to

$$\left[F_1'(a)/F_1(a)\right]^2 - (m/x)^2 = 0 \tag{7}$$

where

$$x = k_{\rho 1}a.$$

The solutions of this equation are

$$J_{m-1}(x_0^+) = 0 \qquad \text{for } EH_{mn}^{MS} \tag{8}$$

$$J_{m+1}(x_0^-) = 0 \qquad \text{for } EH_{-mn}^{MS}. \tag{9}$$

Superscript MS indicates the notation by Marcatili and Schmeltzer [5]. This superscript is used to distinguish this notation from the conventional notation. In this case, the field distributions are also simplified. Equations (6) (or equivalent (5)) in this limit becomes

$$A/B = +1 \qquad \text{for } EH_{mn}^{MS} \tag{10}$$

$$A/B = -1 \qquad \text{for } EH_{-mn}^{MS} \tag{11}$$

and the modal fields in the air region are given by

$$E_\rho = -BJ_{m-1}(k_{\rho 0}^{+}\rho)\cos m\phi, \qquad H_\rho = -Y_0 E_\phi \quad (12a)$$

$$E_\phi = BJ_{m-1}(k_{\rho 0}^{+}\rho)\sin m\phi, \qquad H_\phi = Y_0 E_\rho \quad (12b)$$

$$E_z = H_z = 0 \qquad \text{for } \mathrm{EH}_{mn}^{\mathrm{MS}} \quad (12c)$$

$$E_\rho = -BJ_{m+1}(k_{\rho 0}^{-}\rho)\cos m\phi, \qquad H_\rho = -Y_0 E_\phi \quad (13a)$$

$$E_\phi = -BJ_{m+1}(k_{\rho 0}^{-}\rho)\sin m_\phi, \qquad H_\phi = Y_0 E_\rho \quad (13b)$$

$$E_z = H_z = 0 \qquad \text{for } \mathrm{EH}_{-mn}^{\mathrm{MS}} \quad (13c)$$

where

$$k_{\rho 0}^{+} = x_0^{+}/a, \qquad k_{\rho 0}^{-} = x_0^{-}/a.$$

Here x_0^{+} and x_0^{-} are given in (8) and (9), respectively, and B is a constant. The fields in the lossy region are vanishingly small. The field diagrams of the $\mathrm{EH}_{mn}^{\mathrm{MS}}$ and $\mathrm{EH}_{-mn}^{\mathrm{MS}}$ modes in the air region are shown in Fig. 2 in [5].

When a/λ is large but finite, the attenuation constants of the normal modes are small and the fields decay very rapidly from the interface to the lossy layer. In this case, the asymptotic forms of the Bessel functions can be used for the field functions in the lossy region. The characteristic function of (1) in this approximation is then simplified to

$$[xF_1'(a)/F_1(a)]^2 + jx[xF_1'(a)/F_1(a)](k_{\rho 1}/k_{\rho 2}) \cdot(\epsilon_2+\mu_2) - m^2 - x^2\epsilon_2\mu_2(k_{\rho 1}/k_{\rho 2})^2 = 0 \quad (14)$$

where $x = k_{\rho 1}a$

Suppose $x = x_0 + \Delta x$ where x_0 is the solution as a/λ becomes infinite. Taking the first-order terms in $k_{\rho 1}/k_{\rho 2}$ of the above equation, the attenuation constant is given by

$$\alpha_{mn} = \left(\frac{\xi_{mn}}{2\pi}\right)^2 \frac{\lambda^2}{a^3}\,\mathrm{Re}(\nu_n) \quad (15a)$$

where

$$\nu_n = \begin{cases} \epsilon_2/\sqrt{\epsilon_2\mu_2 - 1} & \text{for } \mathrm{TM}_{0n} \text{ modes } (m=0) \quad (15b)\\ \mu_2/\sqrt{\epsilon_2\mu_2 - 1} & \text{for } \mathrm{TE}_{0n} \text{ modes } (m=0) \quad (15c)\\ \frac{1}{2}(\epsilon_2+\mu_2)/\sqrt{\epsilon_2\mu_2-1} & \\ \quad \text{for } \mathrm{EH}_{mn}^{\mathrm{MS}} \text{ and } \mathrm{EH}_{-mn}^{\mathrm{MS}}\ (m \neq 0). & (15d) \end{cases}$$

Here ξ_{mn} is the solution of

$$J_0'(\xi_{0n}) = 0 \qquad \text{for } \mathrm{TM}_{0n} \text{ and } \mathrm{TE}_{0n} \text{ modes } (m=0) \quad (15e)$$

$$J_{m-1}(\xi_{mn}) = 0 \qquad \text{for } \mathrm{EH}_{mn}^{\mathrm{MS}} \text{ modes } (m \neq 0) \quad (15f)$$

$$J_{m+1}(\xi_{mn}) = 0 \qquad \text{for } \mathrm{EH}_{-mn}^{\mathrm{MS}} \text{ modes } (m \neq 0). \quad (15g)$$

This is almost the same as the result of Marcatili and Schmeltzer except that the coating material is not restricted to a dielectric but can be magnetic as well.

For the first-order approximation of the attenuation constant with $m \neq 0$, we neglected the last term of (14). Even though this term is of the second order in $k_{\rho 1}/k_{\rho 2}$, the coefficient $|x^2\epsilon_2\mu_2|$ can be a large number for the higher-order modes. Thus we expect that the agreement between our exact solution and the first-order solution requires a larger value of a/λ for a higher-order mode (more discussion is given in Section IV).

B. Surface Mode

When the coating material is not lossy enough, some of the normal modes become surface modes. The fields of those modes are confined within the thin layer of the coating and the propagation constants are nearly independent of the inner radius a. When a/λ is sufficiently large, the characteristic equation is approximated to

$$\left[1+\epsilon_2\frac{jk_{\rho 1}}{k_{\rho 2}}\cot(k_{\rho 2}\tau)\right]\left[1-\mu_2\frac{jk_{\rho 1}}{k_{\rho 2}}\tan(k_{\rho 2}\tau)\right] = 0 \quad (16)$$

where τ is the layer thickness, $b-a$. Assuming $|k_{\rho 1}| \gg k_0$, we obtain

$$k_z = \begin{cases} \left[\epsilon_2\mu_2 k_0^2 - \{(n-\frac{1}{2})\pi/\tau\}^2\right]^{1/2} & \\ \quad \text{for } \mathrm{TM}_{mn}^{su} & (17)\\ \left[\epsilon_2\mu_2 k_0^2 - (n\pi/\tau)^2\right]^{1/2} \quad \text{for } \mathrm{TE}_{mn}^{su} & (18) \end{cases}$$

where $n = 1,2,3,\cdots$.

Superscript su indicates the surface mode. The fields in Region II in this limit can be approximately shown to be

$$E_\rho = C_1\cos k_{\rho 2}(b-\rho) \quad (19a)$$

$$E_z = -jC_1(k_{\rho 2}/k_z)\sin k_{\rho 2}(b-\rho) \quad (19b)$$

$$H_\phi = C_1Y_2(k_2/k_z)\cos k_{\rho 2}(b-\rho) \quad (19c)$$

$$E_\phi = H_\rho = H_z = 0 \qquad \text{for } \mathrm{TM}_{mn}^{su} \quad (19d)$$

$$E_\phi = D_1\sin k_{\rho 2}(b-\rho) \quad (20a)$$

$$H_\rho = -D_1Y_2(k_z/k_2)\sin k_{\rho_2}(b-\rho) \quad (20b)$$

$$H_z = -jD_1Y_2(k_{\rho 2}/k_2)\cos k_{\rho 2}(b-\rho) \quad (20c)$$

$$E_\rho = E_z = H_\phi = 0 \qquad \text{for } \mathrm{TE}_{mn}^{su} \quad (20d)$$

where C_1 and D_1 are constants. Thus, the TE_{mn}^{su} mode can be approximated by a normal mode between two PEC slabs and the TM_{mn}^{su} mode by a normal mode between PMC and PEC slabs. The correspondence between the normal modes in a thinly coated waveguide and the surface modes is not unique but depends on the type of coating material. When the coating material is lossless, the $\mathrm{HE}_{mn}(\mathrm{EH}_{mn})$ modes become $\mathrm{TM}_{mn}^{su}(\mathrm{TE}_{mn}^{su})$ (except $m=0$) as the layer thickness increases. The normal modes with $m=0$ are pure TE or TM as indicated in Section II.

C. Interface Mode

There exists an "interface" mode, which is unique to the waveguide coated with a lossy material. The interface mode has large fields near the interface between the air and lossy regions, and the fields decay exponentially to both sides of the interface. Since the fields are limited to the interface region, the attenuation constant is independent of the waveguide's radius. As a/λ is sufficiently large and the coating material is sufficiently lossy, the characteristic equation for the interface mode is well-approximated to

$$(1-\epsilon_2 k_{\rho 1}/k_{\rho 2})(1-\mu_2 k_{\rho 1}/k_{\rho 2})=0. \quad (21)$$

The propagation constants are then evaluated to be

$$k_z=\begin{cases} k_0\left[(\epsilon_2^2-\epsilon_2\mu_2)/(\epsilon_2^2-1)\right]^{1/2} & \text{for TM}^{\text{in}} \quad (22)\\ k_0\left[(\mu_2^2-\epsilon_2\mu_2)/(\mu_2^2-1)\right]^{1/2} & \text{for TE}^{\text{in}}. \quad (23)\end{cases}$$

The modal fields are given by

$$E_\rho^I=C_2\exp\left[jk_{\rho 1}(a-\rho)\right],$$
$$E_\rho^{II}=(C_2/\epsilon_2)\exp\left[-jk_{\rho 2}(\rho-a)\right] \quad (24a)$$
$$E_z^I=-(k_{\rho 1}/k_z)E_\rho^I,$$
$$E_z^{II}=-(k_{\rho 2}/k_z)E_\rho^{II} \quad (24b)$$
$$H_\phi^I=(Y_0k_0/k_z)E_\rho^I,$$
$$H_\phi^{II}=(Y_2k_2/k_z)E_\rho^{II} \quad \text{for TM}^{\text{in}} \quad (24c)$$
$$E_\phi^I=D_2\exp\left[jk_{\rho 1}(a-\rho)\right],$$
$$E_\phi^{II}=D_2\exp\left[-jk_{\rho 2}(\rho-a)\right] \quad (25a)$$
$$H_\rho^I=-(Y_0k_z/k_0)E_\phi^I,$$
$$H_\rho^{II}=-(Y_2k_z/k_2)E_\phi^{II} \quad (25b)$$
$$H_z^I=(Y_0k_{\rho 1}/k_0)E_\phi^I,$$
$$H_z^{II}=(Y_2k_{\rho 2}/k_2)E_\phi^{II} \quad \text{for TE}^{\text{in}} \quad (25c)$$

where all other field components vanish and C_2 and D_2 are constants. Here superscript in indicates the interface mode. From the above results, we can see that the interface mode is well-approximated to the normal mode on the surface of a semi-infinite lossy material [12], [13].

There exist two interface modes at most. The fields of the interface mode decay rapidly to both sides of the interface. The conditions for the interface mode to exist are easily recognized from (24) and (25) to be

$$Im(k_{\rho 1}a)\gg 1 \quad (26)$$

and

$$-Im(k_{\rho 2}\tau)\gg 1. \quad (27a)$$

Using the boundary conditions at the interface, (27a) can be rewritten equivalently as either

$$-Im(k_{\rho 1}\epsilon_2\tau)\gg 1 \quad \text{for TM}^{\text{in}} \quad (27b)$$

or

$$-Im(k_{\rho 1}\mu_2\tau)\gg 1 \quad \text{for TE}^{\text{in}}. \quad (27c)$$

Thus for dielectric coating, only TM$^{\text{in}}$ of the two modes can exist, and only the TE$^{\text{in}}$ mode can be excited in a waveguide coated with a magnetic material.

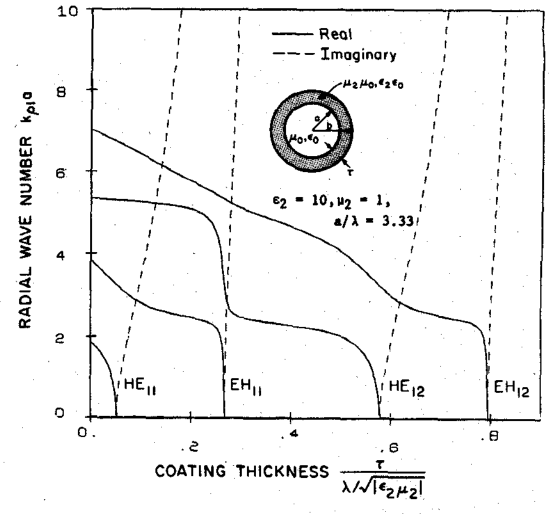

Fig. 10. Radial wave numbers of the normal modes in a waveguide coated with lossless dielectric material ($\epsilon_2=10$, $\mu_2=1$, $a/\lambda=3.33$).

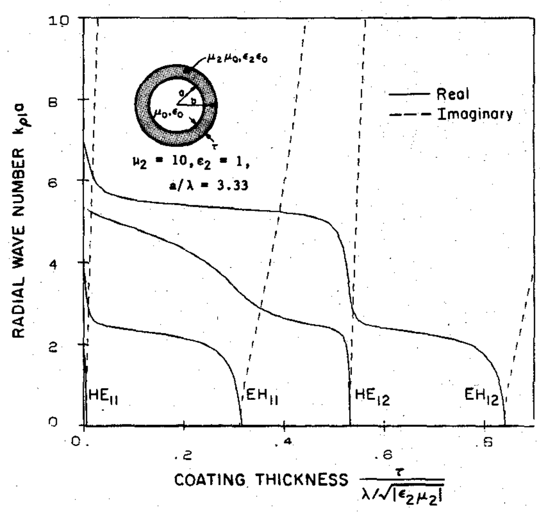

Fig. 11. Radial wave numbers of the normal modes in a waveguide coated with a lossless magnetic material ($\mu_2=10$, $\epsilon_2=1$, $a/\lambda=3.33$).

IV. Numerical Results and Discussion

A. Lossless Coating

When the coating material is lossless, the normal modes in the overmoded coated waveguide become surface waves as the layer thickness increases, in the order of $HE_{m1}, EH_{m1}, HE_{m2}, EH_{m2}, \cdots$ $(m\neq 0)$ and $EH_{01}, HE_{01}, EH_{02}, HE_{02}, \cdots$ $(m=0)$ [4]. These features of the normal modes are shown in Fig. 10 (Fig. 11) for a dielectric (magnetic) coating, where the radial wave numbers are plotted as a function of the layer thickness. The large imaginary part of a complex radial number indicates that the modal field shifts to the waveguide wall and the mode behaves as a surface mode. Note that the HE_{11} in the magnetic-coated guide becomes a surface mode with a much thinner coating layer than that in the dielectric-coated guide. Otherwise, the onset of a new surface mode occurs around every quarter-wavelength thickness as the layer thickness increases.

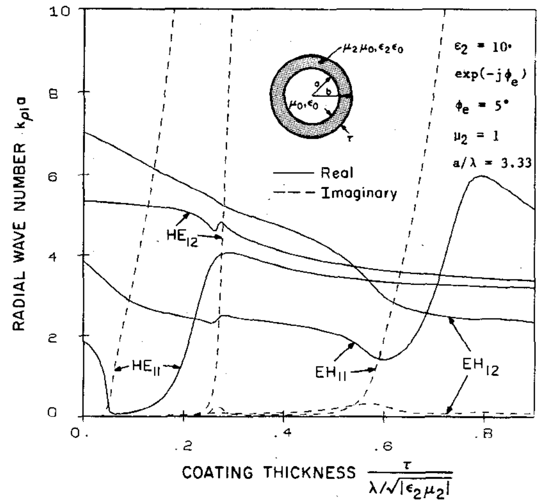

Fig. 12. Radial wave numbers of the normal modes in a circular waveguide coated with a lossy dielectric material ($\epsilon_2 = 10\exp(-j\phi_e)$, $\phi_e = 5°$, $\mu_2 = 1$, $a/\lambda = 3.33$).

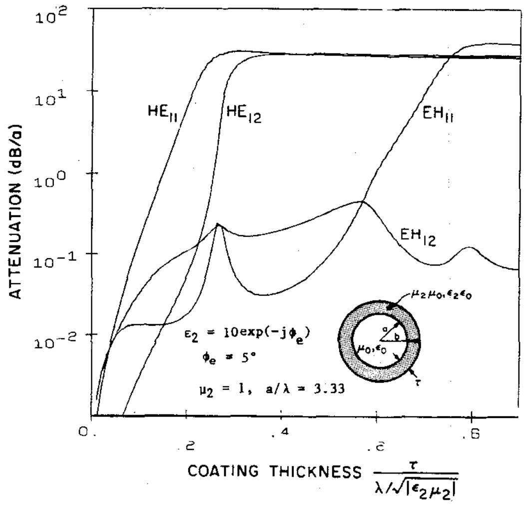

Fig. 14. Attenuation constants of the normal modes in a circular waveguide coated with a lossy dielectric material ($\epsilon_2 = 10\exp(-j\phi_e)$, $\phi_e = 5°$, $\mu_2 = 1$, $a/\lambda = 3.33$).

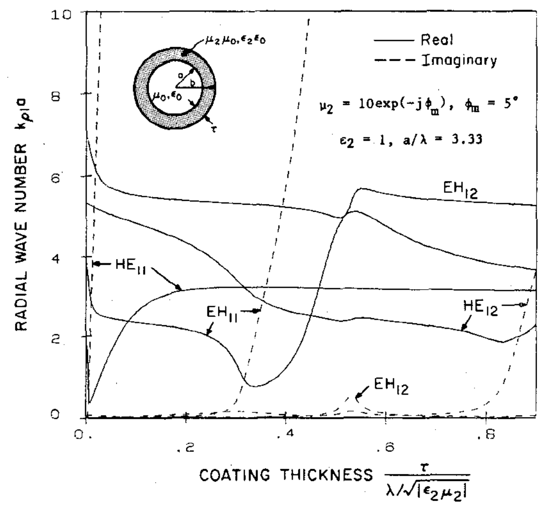

Fig. 13. Radial wave numbers of the normal modes in a circular waveguide coated with a lossy magnetic material ($\mu_2 = 10\exp(-j\phi_m)$, $\phi_m = 5°$, $\epsilon_2 = 1$, $a/\lambda = 3.33$).

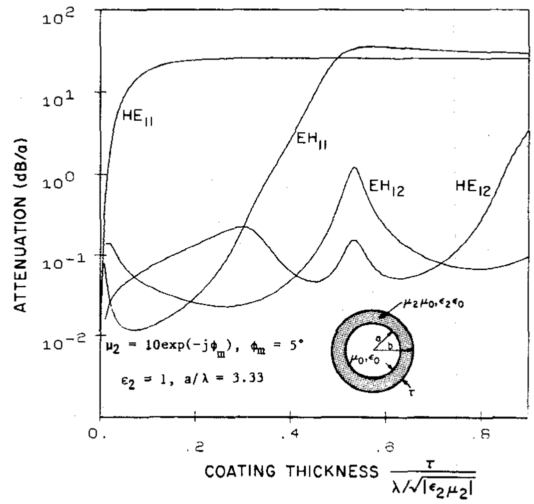

Fig. 15. Attenuation constants of the normal modes in a circular waveguide coated with a lossy magnetic material ($\mu_2 = 10\exp(-j\phi_m)$, $\phi_m = 5°$, $\epsilon_2 = 1$, $a/\lambda = 3.33$).

B. Slightly Lossy Coating

Fig. 12 (Fig. 13) shows the radial wave numbers of the normal modes in a circular guide coated with a slightly lossy dielectric (magnetic) material. The general trend of the normal mode with variation of the layer thickness remains similar to that for the waveguide coated with a lossless material (Figs. 10 and 11). As shown in Figs. 14 and 15, the mode with a large imaginary part of the complex radial number of a surface-wave type has a large attenuation constant. This is due to the fact that the surface mode has a large field concentration within the lossy region near the waveguide wall. It is interesting to note that the HE_{11} mode in the magnetic-coated guide acquires a very large attenuation constant with a much thinner coating layer than that in the dielectric-coated guide. The higher-order modes also become surface modes and acquire large attenuation constants only at a much thicker coating layer.

C. Very Lossy Coating

When the coating material becomes very lossy, those features of the normal modes in the waveguide coated with a lossless material disappear. In fact, the propagation constant of the normal mode is independent of the layer thickness if the lossy layer is thicker than the skin depth of the normal mode (Figs. 16 and 17). There is a mode separation between highly attenuated and lowly attenuated low-order modes. The highly attenuated modes in a dielectric-coated guide are usually lowly attenuated modes in a magnetic-coated guide and vice versa (Figs. 18 and 19). In general, the mode separation is less distinctive for higher-order modes.

When a/λ is large and the coating material is lossy enough, most of the low-order modes are inner modes which are mainly confined in the air region and the attenuation constants are small. Marcatili and Schmeltzer [5] evaluated the attenuation constants using the perturba-

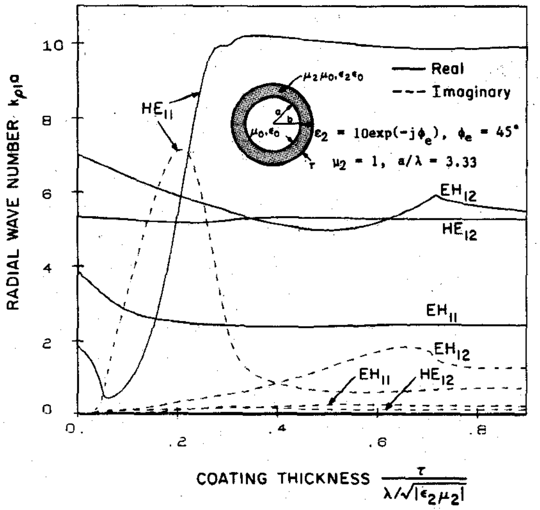

Fig. 16. Radial wave numbers of the normal modes in a circular waveguide coated with a lossy dielectric material ($\epsilon_2 = 10\exp(-j\phi_e)$, $\phi_e = 45°$, $\mu_2 = 1$, $a/\lambda = 3.33$).

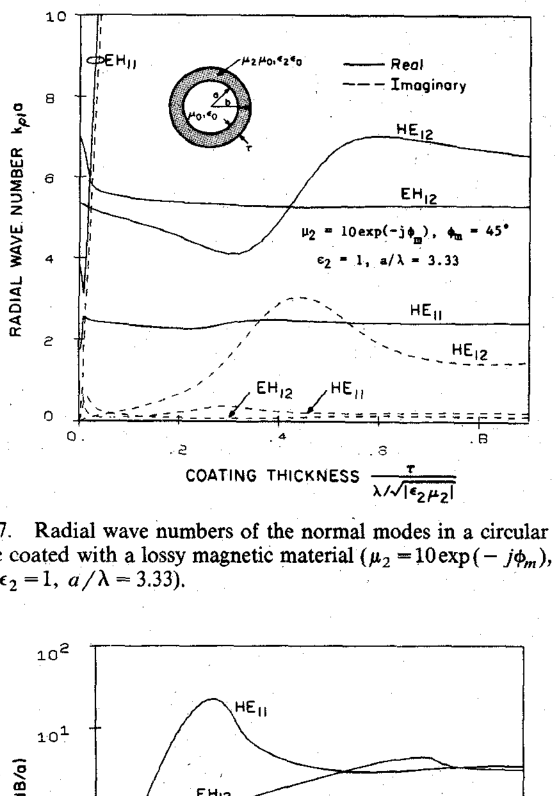

Fig. 17. Radial wave numbers of the normal modes in a circular waveguide coated with a lossy magnetic material ($\mu_2 = 10\exp(-j\phi_m)$, $\phi_m = 45°$, $\epsilon_2 = 1$, $a/\lambda = 3.33$).

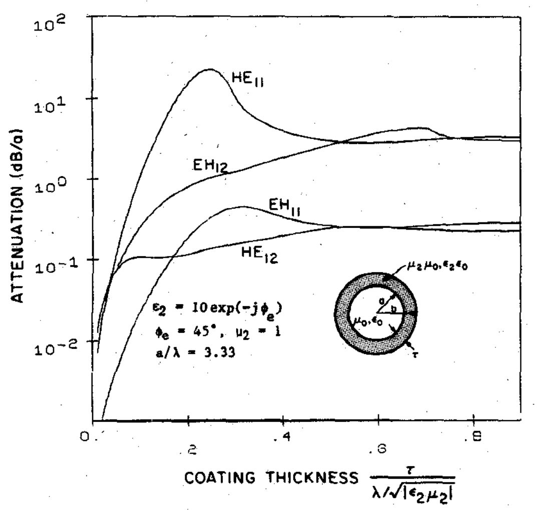

Fig. 18. Attenuation constants of the normal modes in a circular waveguide coated with a lossy dielectric material ($\epsilon_3 = 10\exp(-j\phi_e)$, $\phi_e = 45°$, $\mu_2 = 1$, $a/\lambda = 3.33$).

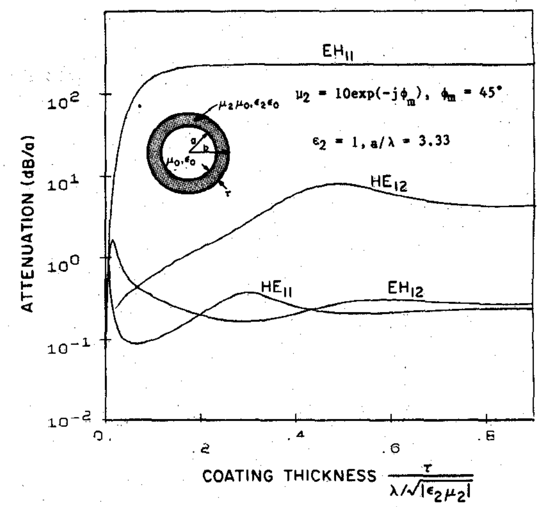

Fig. 19. Attenuation constants of the normal modes in a circular waveguide coated with a lossy magnetic material ($\mu_2 = 10\exp(-j\phi_m)$, $\phi_m = 45°$, $\epsilon_2 = 1$, $a/\lambda = 3.33$).

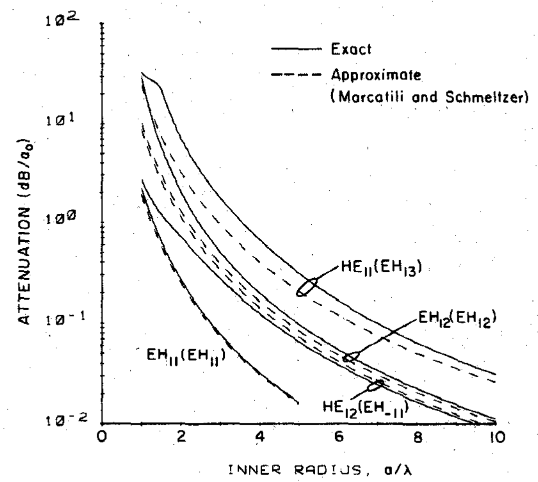

Fig. 20. Attenuation constants of the normal modes as a function of the inner radius a, with a fixed layer thickness ($\tau = 0.949\lambda\sqrt{|\epsilon_2\mu_2|}$) in a circular waveguide coated with a lossy dielectric material ($\epsilon_2 = 10\exp(-j\phi_e)$, $\phi_e = 45°$, $\mu_2 = 1$, $a_0/\lambda = 3.33$). The mode names in the parentheses correspond to those in Marcatili and Schmeltzer's paper [5].

tion theory under the assumption that a/λ is large and the fields within the lossy region are small (see Section III). Fig. 20 shows the comparison of the exact solutions with the approximate solutions by Marcatili and Schmeltzer for the attenuation constants of the normal modes in a dielectric-coated guide. Here the coating thickness τ is fixed while a/λ is varied. We note that the exact and approximate solutions are in better agreement at a larger value of a/λ. The high-order modes usually require a large value of a/λ for good agreement between the exact and approximate solutions (see Section III-A). This result indicates that the low-order modes become excluded from the lossy layer near the wall at a smaller value of a/λ than do the high-order modes.

Fig. 21 shows the comparison of the exact and various approximate solutions for the attenuation constants of the normal modes in a magnetic-coated circular guide. Most of the low-order modes become inner modes at a large value

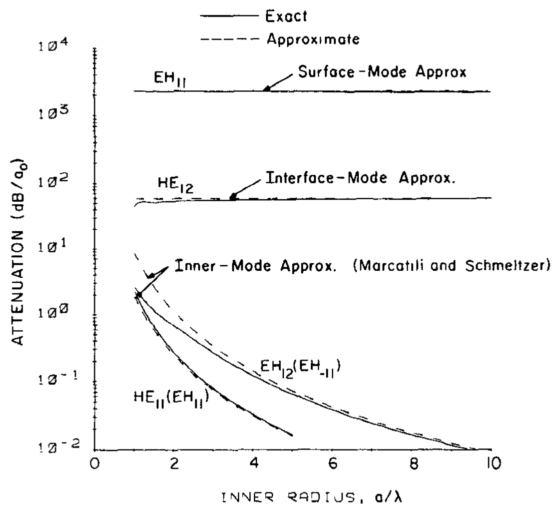

Fig. 21. Attenuation constants of the normal modes as a function of the inner radius a, with a fixed layer thickness ($\tau = 0.949\lambda/\sqrt{|\epsilon_2 \mu_2|}$) in a circular waveguide coated with a lossy magnetic material ($\mu_2 = 10\exp(-j\phi_m)$, $\phi_m = 45°$, $\epsilon_2 = 1$, $a_0/\lambda = 3.33$). The mode names in the parentheses correspond to those in Marcatili and Schmeltzer's paper [5].

of a/λ as in the case of the dielectric coating (Fig. 20). However, certain modes are confined near the wall. The EH_{11} mode at a large a/λ becomes a surface mode (Section III-B), whose fields are mainly confined within the lossy region and have a large attenuation constant. The exact solution of the attenuation constant is well-approximated by the solution for the surface mode given in (17). The existence of the surface mode in a waveguide coated with a lossy material depends on whether the characteristic equation (16) has a solution close to the value for a surface mode (17) or (18). Also note that the HE_{12} mode becomes an interface mode (Section III-C) whose fields are limited to the region near the interface between the air and lossy material. The attenuation constant of the interface mode is well-approximated by that of the mode on the surface of a semi-infinite lossy material. The criteria for the existence of the interface modes in a coated guide are given in (26) and (27). Thus, the attenuation constant of the interface mode is not as large as that of the surface mode but much larger than that of the inner mode (Fig. 21).

In Figs. 20 and 21, the mode names in the parentheses for the inner modes correspond to the mode names by Marcatili and Schmeltzer [5], where the field diagrams of those modes are also shown. The surface mode does not exist when the lossy layer becomes infinitely extended. However, the interface mode should exist in a hollow lossy circular guide if the conditions in (26) and (27) are satisfied.

D. Mode Suppressor

So far, we have seen that the attenuation properties of the normal modes in a coated waveguide depend on the coating material, layer thickness, and frequency. When the coating material is not very lossy, the attenuation constants of the normal modes strongly vary with the layer thickness. Since each mode has its own region where the mode is significantly attenuated, the coated guide can be used as a simple mode suppressor [14]. The device will be especially useful for eliminating low-order modes. Since low-order modes are mainly responsible for the radar cross section (RCS) at a small incident angle from a cavity-type structure, coating the cavity wall with a lossy material will be effective in reducing the RCS due to the undesirable interior irradiation from the normal modes in a cavity [15], [16]. In a practical design, the transition region between the uncoated and coated sections of the waveguide must be long enough to prevent any mode conversion [17].

E. CP Antenna

When the coating material is sufficiently lossy and a/λ is large, most of the normal modes become inner modes if the coating layer is thick enough, i.e., thicker than the skin depths of the modal fields. Both the magnetic and electric fields of the inner mode are small near the waveguide wall. The HE_{11} mode in the waveguide coated with a lossy magnetic material becomes an inner mode at a much smaller value of a/λ than that with a lossy dielectric material. The boundary conditions of the HE_{11} mode in this case are similar to those of a corrugated waveguide [18]–[21]; hence, this waveguide can be used as an alternate to the corrugated waveguide to produce circularly polarized radiation or reduce the side-lobe level. Even though the loss of the HE_{11} mode in the coated waveguide may be higher than that of a well-designed corrugated waveguide, the coated waveguide is cheaper to build and lighter in weight than the corrugated waveguide, as explained in [22].

V. Conclusion

The normal modes in a circular guide coated with a lossy material are classified and analyzed, emphasizing the attenuation properties of the normal modes. It is shown that the coating material should not be too lossy for the low-order modes to be significantly attenuated. A much thinner coating layer is required for the attenuation of the HE_{11} mode when the coating material is magnetic rather than dielectric. The coating technique is especially useful in reducing the radar cross section from a jet engine inlet, a subject that will be reported by us in a future communication.

When a/λ is large and the coating material is very lossy, most of the low-order modes become inner modes, which have small fields within the lossy region and small attenuation constants. An interesting application of the HE_{11} mode in an open-ended waveguide coated with a very lossy magnetic material is that it can be used for circularly polarized radiation [22].

APPENDIX I
DEGENERACY BETWEEN THE CUTOFF FREQUENCIES OF THE TM_{11} AND TE_{01} MODES IN A DIELECTRIC-COATED CIRCULAR WAVEGUIDE

At the cutoff frequency ($k_z = 0$), the characteristic equation in (1) becomes

$$\begin{aligned} &J_1'(k_{CM}a)[J_1(k_{CM2}a)N_1(k_{CM2}b) \\ &\quad - N_1(k_{CM2}a)J_1(k_{CM2}b)] \\ &\quad - \sqrt{\epsilon_2/\mu_2}J_1(k_{CM}a)[J_1'(k_{CM2}a)N_1(k_{CM2}b) \\ &\quad - N_1'(k_{CM2}a)J_1(k_{CM2}b)] = 0 \qquad \text{for } TM_{11} \quad \text{(A1-1)} \end{aligned}$$

or

$$\begin{aligned} &J_0'(k_{CE}a)[J_0(k_{CE2}a)N_0'(k_{CE2}b) \\ &\quad - N_0(k_{CE2}a)J_0'(k_{CE2}b)] \\ &\quad - \sqrt{\mu_2/\epsilon_2}J_0(k_{CE}a)[J_0'(k_{CE2}a)N_0'(k_{CE2}b) \\ &\quad - N_0'(k_{CE2}a)J_0'(k_{CE2}b)] = 0 \qquad \text{for } TE_{01} \quad \text{(A1-2)} \end{aligned}$$

where

$$k_{CM} = \frac{2\pi}{c}f_{CM}, \qquad k_{CM2} = k_{CM}\sqrt{\epsilon_2\mu_2}$$

$$k_{CE} = \frac{2\pi}{c}f_{CE}, \qquad k_{CE2} = k_{CE}\sqrt{\epsilon_2\mu_2}.$$

Here f_{CM} and f_{CE} are the cutoff frequencies for the TM_{11} and TE_{01} modes, respectively.

Using the recurrence relations of Bessel functions [23], the derivative expressions in (A1-1) and (A1-2) can be eliminated, and we obtain

$$\begin{aligned} &J_1(k_{CM}a)[J_0(k_{CM2}a)N_1(k_{CM2}b) \\ &\quad - N_0(k_{CM2}a)J_1(k_{CM2}b)] \\ &\quad - \left[\sqrt{\mu_2/\epsilon_2}J_0(k_{CM}a) - \left(1/\sqrt{\epsilon_2\mu_2} - \sqrt{\mu_2/\epsilon_2}\right)/k_{CM}a\right] \\ &\quad \cdot [J_1(k_{CM2}a)N_1(k_{CM2}b) \\ &\quad - N_1(k_{CM2}a)J_1(k_{CM2}b)] = 0 \qquad \text{for } TM_{11} \quad \text{(A1-3)} \end{aligned}$$

and

$$\begin{aligned} &J_1(k_{CE}a)[J_0(k_{CE2}a)N_1(k_{CE2}b) \\ &\quad - N_0(k_{CE2}a)J_1(k_{CE2}b) \\ &\quad - \sqrt{\mu_2/\epsilon_2}J_0(k_{CE}a)[J_1(k_{CE2}a)N_1(k_{CE2}b) \\ &\quad - N_1(k_{CE2}a)J_1(k_{CE2}b)] = 0 \qquad \text{for } TE_{01}. \quad \text{(A1-4)} \end{aligned}$$

When $\mu_2 = 1$, the two characteristic equations are identical, and the cutoff frequencies of the TM_{11} and TE_{01} modes are the same. On the other hand, when the coating material is magnetic ($\mu_2 \neq 1$), the degeneracy of these two modes at their cutoff frequencies is not present.

APPENDIX II
FIELDS OF THE NORMAL MODES IN A COATED CIRCULAR GUIDE WHEN $k_{\rho 1} = 0$ (DIRECT METHOD)

From Maxwell's equations, we obtain four equations for the normal modes in a circular guide

$$\nabla \times \nabla \times \vec{E} - k_0^2\vec{E} = 0 \qquad \text{(A2-1a)}$$

$$\nabla \cdot \vec{E} = 0. \qquad \text{(A2-1b)}$$

First consider the case for $m \neq 0$. Due to the symmetry of the problem, we can assume that

$$E_\rho = R_\rho(\rho)\cos m\phi\, e^{-jk_z z} \qquad \text{(A2-2a)}$$

$$E_\phi = R_\phi(\rho)\sin m\phi\, e^{-jk_z z} \qquad \text{(A2-2b)}$$

$$E_z = R_z(\rho)\cos m\phi\, e^{-jk_z z}. \qquad \text{(A2-2c)}$$

Since $k_{\rho 1} = 0$, from the dispersion relation

$$k_z = k_0. \qquad \text{(A2-3)}$$

Substituting (A2-2) in (A2-1), three linearly independent equations are obtained

$$\rho\frac{d}{d\rho}\left[\rho\left(\frac{dR_z(\rho)}{d\rho}\right)\right] - m^2R_z(\rho) = 0 \quad \text{(A2-4a)}$$

$$m\frac{d}{d\rho}[\rho R_\phi(\rho)] + m^2R_\rho(\rho) - jk_0\rho^2\frac{dR_z(\rho)}{d\rho} = 0 \quad \text{(A2-4b)}$$

$$\frac{d}{d\rho}[\rho R_\rho(\rho)] + mR_\phi(\rho) - jk_0\rho R_z(z) = 0. \quad \text{(A2-4c)}$$

Solving these coupled equations, the fields in Region I ($m \neq 0$) are given by

$$E_\rho^I = \left(C_1\rho^{m+1} + C_2\rho^{m-1}\right)\cos m\phi \qquad \text{(A2-5a)}$$

$$E_\phi^I = \left(C_1\rho^{m+1} - C_2\rho^{m-1}\right)\sin m\phi \qquad \text{(A2-5b)}$$

$$E_z^I = \frac{2(m+1)C_1}{jk_0}\rho^m\cos m\phi \qquad \text{(A2-5c)}$$

$$H_\rho^I = -Y_0\left[C_1\rho^{m+1} + \left(\frac{2m(m+1)C_1}{k_0^2} - C_2\right)\rho^{m-1}\right]\sin m\phi \qquad \text{(A2-5d)}$$

$$H_\phi^I = Y_0\left[C_1\rho^{m+1} - \left(\frac{2m(m+1)C_1}{k_0^2} - C_2\right)\rho^{m-1}\right]\cos m\phi \qquad \text{(A2-5e)}$$

$$H_z^I = -Y_0\frac{2(m+1)C_1}{jk_0}\rho^m\sin m\phi. \qquad \text{(A2-5f)}$$

Using (A2-3), the fields in Region II ($m \neq 0$) are obtained from (2)

$$E_\rho^{II} = -\left[\frac{D_1}{\sqrt{\epsilon_2\mu_2}}G_3'(\rho) + \frac{D_2m}{k_{\rho 2}\rho}G_4(\rho)\right]\cos m\phi \qquad \text{(A2-6a)}$$

$$E_\phi^{II} = \left[\frac{D_1m}{\sqrt{\epsilon_2\mu_2}\,k_{\rho 2}\rho}G_3(\rho) + D_2G_4'(\rho)\right]\sin m\phi \qquad \text{(A2-6b)}$$

$$E_z^{II} = \frac{D_1 k_{\rho 2}}{jk_2} G_3(\rho) \cos m\phi \quad \text{(A2-6c)}$$

$$H_\rho^{II} = -Y_2 \left[\frac{D_1 m}{k_{\rho 2}\rho} G_3(\rho) + \frac{D_2}{\sqrt{\epsilon_2 \mu_2}} G_4'(\rho) \right] \sin m\phi \quad \text{(A2-6d)}$$

$$H_\phi^{II} = -Y_2 \left[D_1 G_3'(\rho) + \frac{D_2 m}{\sqrt{\epsilon_2 \mu_2}\, k_{\rho 2}\rho} G_4(\rho) \right] \cos m\phi \quad \text{(A2-6e)}$$

$$H_z^{II} = Y_2 \frac{D_2 k_{\rho 2}}{jk_2} G_4(\rho) \sin m\phi \quad \text{(A2-6f)}$$

where

$$G_3(\rho) = J_m(k_{\rho 2}\rho) N_m(k_{\rho 2}b) - N_m(k_{\rho 2}\rho) J_m(k_{\rho 2}b) \quad \text{(A2-6g)}$$

$$G_3'(\rho) = J_m'(k_{\rho 2}\rho) N_m(k_{\rho 2}b) - N_m'(k_{\rho 2}\rho) J_m(k_{\rho 2}b) \quad \text{(A2-6h)}$$

$$G_4(\rho) = J_m(k_{\rho 2}\rho) N_m'(k_{\rho 2}b) - N_m(k_{\rho 2}\rho) J_m'(k_{\rho 2}b) \quad \text{(A2-6i)}$$

$$G_4'(\rho) = J_m'(k_{\rho 2}\rho) N_m'(k_{\rho 2}b) - N_m'(k_{\rho 2}\rho) J_m'(k_{\rho 2}b). \quad \text{(A2-6j)}$$

Note that the convention of $e^{j(\omega t - k_0 z)}$ is understood and omitted. Here $k_{\rho 2} = \sqrt{\epsilon_2 \mu_2 - 1}\, k_0$, and C_1, C_2, D_1, and D_2 are constants to be determined by imposing the boundary conditions at the interface between the air and material regions. These constants are related by

$$C_1 = \frac{G_3(a) k_{\rho 2} D_1}{\sqrt{\epsilon_2 \mu_2}\, 2(m+1) a^m} \quad \text{(A2-7a)}$$

$$D_2 = -\sqrt{\mu_2/\epsilon_2}\, \frac{G_3(a)}{G_4(a)} D_1 \quad \text{(A2-7b)}$$

$$C_2 = a^2 C_1 - \left[\frac{D_1 m G_3(a)}{\sqrt{\epsilon_2 \mu_2}\, k_{\rho 2} a} + D_2 G_4'(a) \right] \Big/ a^{m-1}. \quad \text{(A2-7c)}$$

The coating thickness is determined by the characteristic equation

$$\frac{(k_{\rho 2}a)^2}{m+1} + (k_{\rho 2}a) \left[\frac{G_3'(a)}{G_3(a)} \epsilon_2 + \frac{G_4'(a)}{G_4(a)} \mu_2 \right] - m(\epsilon_2 \mu_2 + 1) = 0. \quad \text{(A2-8)}$$

Note that the fields are neither TE nor TM and the fields in Region I do not show a Bessel-function dependence of radial distance.

The fields for $m = 0$ can be similarly shown to be

$$E_\rho^I = \frac{jk_0 C_{10}}{2} \rho, \quad E_\rho^{II} = -\frac{jC_{20}}{\sqrt{\epsilon_2 \mu_2 - 1}} G_{30}'(\rho) \quad \text{(A-9a)}$$

$$H_\phi^I = Y_0 E_\rho^I, \quad H_\phi^{II} = Y_0 \epsilon_2 E_\rho^{II} \quad \text{(A2-9b)}$$

$$E_z^I = C_{10}, \quad E_z^{II} = C_{20} G_{30}(\rho) \qquad \text{for } TM_{0n} \quad \text{(A2-9c)}$$

and

$$H_\rho^I = \frac{jk_0 D_{10}}{2} \rho, \quad H_\rho^{II} = -\frac{jD_{20}}{\sqrt{\epsilon_2 \mu_2 - 1}} G_{40}'(\rho) \quad \text{(A2-10a)}$$

$$E_\phi^I = -H_\rho / Y_0, \quad E_\phi^{II} = -\mu_2 H_\rho^{II} / Y_0 \quad \text{(A2-10b)}$$

$$H_z^I = D_{10}, \quad H_z^{II} = D_{20} G_{40}(\rho) \qquad \text{for } TE_{0n} \quad \text{(A2-10c)}$$

where $G_{30}(\rho)$, $G_{30}'(\rho)$, $G_{40}(\rho)$, and $G_{40}'(\rho)$ are $G_3(\rho)$, $G_3'(\rho)$, $G_4(\rho)$, and $G_4'(\rho)$ with $m = 0$, respectively. All other field components vanish, and C_{10}, C_{20}, D_{10}, and D_{20} are constants which are related by

$$C_{10} = C_{20} G_{30}(a) \quad \text{(A2-11a)}$$

$$D_{10} = D_{20} G_{40}(a). \quad \text{(A2-11b)}$$

The coating thickness for $m = 0$ is determined by the following characteristic equation:

$$G_{30}(a) + \frac{2\epsilon_2}{k_0 a \sqrt{\epsilon_2 \mu_2 - 1}} G_{30}'(a) = 0 \qquad \text{for } TM_{0n} \quad \text{(A2-12a)}$$

or

$$G_{40}(a) + \frac{2\mu_2}{k_0 a \sqrt{\epsilon_2 \mu_2 - 1}} G_{40}'(a) = 0 \qquad \text{for } TE_{0n}. \quad \text{(A2-12b)}$$

The fields are either TE or TM and the fields in the air region show a linear dependence of radial distance instead of the usual Bessel-function dependence in the case of an uncoated guide.

References

[1] M. Miyagi, A. Hongo, and S. Kawakami, "Transmission characteristics of dielectric-coated metallic waveguide for infrared transmission: Slab waveguide model," *IEEE J. Quantum Electron.*, vol. QE-19, pp. 136–145, February 1983.

[2] H. G. Unger, "Lined waveguide," *Bell System Tech. J.*, vol. 41, pp. 745–768, Mar. 1962.

[3] J. W. Carlin and P. D'Agostino, "Low-loss modes in dielectric-lined waveguide," *Bell System Tech. J.*, vol. 50, pp. 1631–1638, May–June 1971.

[4] J. W. Carlin and P. D'Agostino, "Normal modes in overmoded dielectric-lines circular waveguide," *Bell System Tech. J.*, vol. 52, pp. 453–486, Apr. 1973.

[5] E. A. J. Marcatili and R. A. Schmeltzer, "Hollow metallic and dielectric waveguides for long distance optical transmission and lasers," *Bell System Tech. J.*, pp. 1783–1809, July 1964.

[6] C. Dragone, "High-frequency behavior of waveguides with finite surface impedances," *Bell System Tech. J.*, vol. 60, pp. 89–116, Jan. 1981.

[7] P. J. B. Clarricoats, "Propagation along unbounded and bounded dielectric rods," Part 1 and Part 2, *Proc. IEE*, Mon. 409E and 410E, pp. 170–186, October 1960.

[8] G. N. Tsandoulas and W. J. Ince, "Modal inversion in circular waveguides—Part 1: Theory and phenomenology," *IEEE Trans. Microwave Theory Tech.*, vol. MTT-19, pp. 386–392, Apr. 1971.

[9] G. N. Tsandoulas, "Bandwidth enhancement in dielectric-lined circular waveguides," *IEEE Trans. Microwave Theory Tech.*, vol. MTT-21, pp. 651–654, Oct. 1973.

[10] C. S. Lee, S. L. Chuang, S. W. Lee, and Y. T. Lo, "Wave attenuation and mode dispersion in a waveguide coated with lossy dielectric material," Univ. of Illinois Electromagn. Lab., Urbana, IL, Tech. Rep., No. 84-13, July 1984.

[11] R. F. Harrington, *Time Harmonic Electromagnetic Fields.* New York: McGraw-Hill Book Co., 1961.

[12] P. Halevi, "Polariton modes at the interface between two conducting or dielectric media," *Surf. Sci.*, vol. 76, pp. 64–90.

[13] G. N. Zhizhin, M. A. Moskalova, E. V. Shomina, and V. A. Yokovlev, "Surface electromagnetic wave propagation on metal surfaces," in *Surface Polaritons*, by V. M. Agranovich and D. L. Mills, Eds. New York: North-Holland Publishing Co., 1982, pp. 93–144.

[14] T. N. Anderson, "Low-loss transmission using overmoded waveguide, a practical 1981 review of the state of the art," presented at IEEE AP/MTT-S, Philadelphia Section, Benjamin Franklin 1981 Symp. Advances Antenna and Microwave Technol., May 1981.

[15] S. W. Lee, Y. T. Lo, S. L. Chuang, and C. S. Lee, "Numerical methods for analyzing electromagnetic scattering," Semiannual Rep. NASA Lewis Research Center, Cleveland, OH, Mar. 1985.

[16] H. R. Witt and E. L. Price, "Scattering from hollow conducting cylinders," *Proc. IEE*, vol. 115, pp. 94–99, Jan. 1968.

[17] H. Unger, "Circular waveguide taper of improved design," *Bell System Tech. J.*, vol. 37, pp. 899–912, July 1958.

[18] M. J. Al-Hakkak and Y. T. Lo, "Circular waveguide and horns with anisotropic and corrugated boundaries," Antenna Lab. Rep. No. 73-3, Univ. of Illinois, Urbana, IL, 1973.

[19] P. J. B. Clarricoats, A. D. Olver, and S. L. Chong, "Attenuation in corrugated circular waveguide, Part 1, Theory," *Proc. IEE*, vol. 122, pp. 1173–1179, 1975.

[20] C. Dragone, "Reflection and mode conversion in a corrugated feed," *Bell System Tech. J.*, vol. 56, pp. 835–867, 1977.

[21] C. Dragone, "Attenuation and radiation characteristics of the HE mode," *IEEE Trans. Microwave Theory Tech.*, vol. MTT-28, pp. 704–710, 1980.

[22] C. S. Lee, S. L. Chuang, and S. W. Lee, "A simple version of corrugated waveguide: Smooth-walled circular waveguide coated with lossy magnetic material," *AP-S. Int. Symp. Dig.*, vol. 1, pp. 303–306, 1985.

[23] M. Abramowitz and I. A. Stegun, *Handbook of Mathematical Functions*. New York: Dover, 1972.

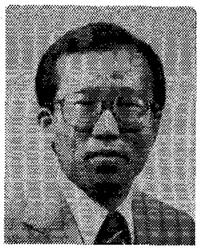

Choon Sae Lee (S'86) was born in Puchon City, Korea, in 1955. He received the B.S. degree from Rice University in 1977 and the M.S. degree from Texas A&M University in 1979, both in physics. At the University of Illinois at Urbana-Champaign, he received the M.S. and Ph.D. degrees in electrical engineering in 1983 and 1986, respectively.

He is currently a visiting assistant professor at the University of Illinois. He served as a teaching assistant in the Departments of Physics of the University of Illinois and Texas A&M University, and a research assistant in the Coordinated Science Laboratory and the Electromagnetics Laboratory of the University of Illinois. His research interests include electromagnetic scattering, microwave devices, and solid-state physics.

He is a member of Eta Kappa Nu, Sigma Pi Sigma, and the American Physical Society.

Shung-Wu Lee (S'83–M'66–SM'73–F'81) was born in Kiangsi, China. He received the B.S. degree in electrical engineering from Cheng Kung University in Tainan, Taiwan, in 1961, and the M.S. and Ph.D. degrees in electrical engineering from the University of Illinois in Urbana.

Currently, he is a professor of electrical and computer engineering and an Associate Director of the Electromagnetics Laboratory at the University of Illinois. He has been on the University's faculty since 1966. While on leave from the University of Illinois, Dr. Lee was with Hughes Aircraft Company, Fullerton, CA, in 1969–1970, and with the Technical University at Eindhoven, The Netherlands, and the University of London, England, 1973–1974.

Dr. Lee has published more than 100 papers in technical journals on antennas and electromagnetic theory. He is the co-author of a book on guided waves published by Macmillan in 1971, and a co-author of an antenna handbook to be published in 1986 by Howard W. Sams and Co.

Dr. Lee received several professional awards, including the 1968 Everitt Teaching Excellence Award from the University of Illinois, 1973 NSF NATO Senior Scientist Fellowship, 1977 Best Paper Award from IEEE Antennas and Propagation Society, and the 1985 Lockheed Million Dollar Award.

Shun-Lien Chuang (S'78–M'82) was born in Taiwan in 1954. He received the B.S. degree in electrical engineering from National Taiwan University in 1976, and the M.S., E.E., and Ph.D. degrees in electrical engineering from the Massachusetts Institute of Technology in 1980, 1981, and 1983, respectively.

While in graduate school, he held research and teaching assistantships, and also served as a recitation instructor. He conducted research at Schlumberger-Doll Research in Ridgefield, CT, during the summers of 1981 and 1982 and also in 1983 as a member of the professional staff. He is now an assistant professor in the Department of Electrical and Computer Engineering at the University of Illinois at Urbana-Champaign. He is conducting research in electromagnetics, millimeter-wave-integrated circuits, and semiconductor devices including the superlattice photodetectors, microwave transistors, and high-electron mobility transistors.

He is a member of the Optical Society of America and the American Physical Society.